A Perceptually Inspired Variational Method for the Uneven Intensity Correction of Remote Sensing Images

Huifang Li, Liangpei Zhang, *Senior Member, IEEE*, and Huanfeng Shen, *Member, IEEE*

***Abstract*—Perceptually inspired color correction methods are characterized by human visual system properties. In this paper, we propose a perceptually inspired variational method for uneven intensity correction of remote sensing images. The proposed method shares the same intrinsic scheme as the Retinex theory, but the reflectance in this method is solved directly within the limited dynamic range and is supposed to comply with the gray world assumption. Considering the smoothness of illumination and the complexity of reflectance, the proposed method integrates L2 norm and total variation prior to inflict varying constraints to different components and regions. The minimum of this variational model is calculated using the steepest descent approach. Experimental results are presented to validate the effectiveness of the proposed method.**

***Index Terms*—Intensity correction, perception, remote sensing images, variational techniques.**

I. Introduction

IN REMOTE sensing image acquisition processes, radiometric errors brought about by internal and external factors are common. Considering the many factors, including the imaging system, the atmosphere status, and other variables in nature, such as terrain elevation, slope, and aspect, we can only ever obtain degraded images of the landscape with uneven intensity distribution, color cast, or other problems. The traditional correction techniques for these degraded images include absolute and relative radiometric correction. Most forms of absolute radiometric correction use a radiative transfer model to correct the imagery; the web-based ACT for Thematic Mapper (TM) and Enhanced Thematic Mapper Plus (ETM+) thermal data adopts MODTRAN-4 code for instance [1]. The application of these models to a satellite scene often requires measurements of the atmosphere and sensor on the acquisition date. For the majority of archived satellite images, these measurement data are not available [2]. When corrected results are not applied in accurate quantitative retrieval, relative radiometric correction, which normalizes an image to a standard one or another referenced one, is often adopted. However, a few studies have attempted to accommodate the uneven illumination and intensity distribution for a single-scene remote sensing image. Several traditional single-scene image enhancement methods can be applied to degraded remote sensing images, such as histogram equalization (HE) and homomorphic filtering. HE is a simple and popular method for image contrast enhancement [3]–[6]. It is, however, simply based on statistical information and independent of location and neighborhoods, and furthermore a unique solution does not exist for multiband HE [7]. By using homomorphic filtering, it is possible to adjust illumination and reflectance separately [8]. However, color distortion usually appears after homomorphic filtering in RGB space [9], [10], and the form of the filter is not unified. These methods are applicable to some specific close-shot images, but do not take enough of the characteristics of remote sensing images into account. A simple intensity correction method, named Mask filtering [11], refers to the uneven illumination as additional noise in an image and subtracts it directly, which is not complying with the imaging system; therefore, the final result usually shows partial blurring and color distortion. This paper focuses on the correction of uneven intensity distribution for a single-scene remote sensing image through perception-inspired variational techniques.

As a kind of visual information, images provide direct stimulus to the human visual system (HVS). The HVS transfers the perceived intensity of the stimuli to the human cortex by nerves; the process of cognition to images is isolated from the environmental illumination. In digital image processing, this characteristic of the HVS has been introduced to some algorithms, namely, perceptually inspired image processing methods. The Retinex theory proposed by Land and McCann in 1971 is the first theory applied to image processing that is based on visual perception [12]. In 1977, Land expounded the Retinex theory and random path algorithm in more detail [13]. After that, researchers confirmed the appropriation of this theory to digital images and developed different path selection strategies [14], [15]. In 1997, Jobson proposed a Retinex version for digital images, named center/surround Retinex, but halo artifacts appeared in the results [16]. A multiscale center/surround Retinex was developed to eliminate these halos [17], but the effect is not pleasing. Ron Kimmel introduced the variational

Manuscript received June 30, 2011; revised July 6, 2011; accepted November 16, 2011. Date of publication January 31, 2012; date of current version July 18, 2012. This work was supported in part by the Major State Basic Research Development Program of China (973 Program) under Grant 2011CB707103 and the National Natural Science Foundation of China under Grants 40930532, 41061130553, and 40801182.

H. Li and L. Zhang are with the State Key Laboratory of Information Engineering in Surveying, Mapping, and Remote Sensing, Wuhan University, Wuhan 430079, China (e-mail: huifang10_lee@yahoo.cn; zlp62@public.wh.hb.cn).

H. Shen is with the School of Resource and Environmental Science and the State Key Laboratory of Information Engineering in Surveying, Mapping, and Remote Sensing, Wuhan University, Wuhan 430079, China (e-mail: shenhf@whu.edu.cn).

Color versions of one or more of the figures in this paper are available online at http://ieeexplore.ieee.org.

Digital Object Identifier 10.1109/TGRS.2011.2178075

Retinex framework [18] in 2003, in which the illumination was firstly extracted from a given image by solving an energy function, and then it was eliminated to result in the recovered lightness. Provenzi discussed the local property of Retinex in 2007 and proposed a 2-D pixel spray to replace the 1-D random path [19].

It is noted that the use of partial differential equations (PDEs) and variational techniques in image processing are becoming more and more common [20]–[22]. In this paper, rather than discussing the properties of these algorithms, we aim to construct an energy function driven by perception to correct the uneven dispersion of remote sensing image intensity. The reason for such a construction is that functional methods allow us to deal with several problems of image processing at the same time and combine different types of algorithms in the framework of PDE or other variational equations [23].

The rest of the paper is organized as follows. In Section II, we review the intrinsic Retinex and its variational framework (VFR). Section III presents the proposed variational correction model, with Section IV describing the experiment results. Section V concludes the paper.

II. Perceptually Inspired Framework: Retinex

In recent years, more attention has been paid to perceptually inspired image processing algorithms, because even though the radiation goes through the same transfer from targets to receiving devices in the HVS and machine systems, the HVS provides us with more abundant knowledge about the scene. This can be attributed to the special properties of HVS: one is locality, that is to say our perception is sensitive to intensity contrast, rather than absolute lightness [23], [24]; the other is color constancy, which means that humans can perceive the colors of a scene almost independent of the spectral electromagnetic composition of a uniform illuminant, usually called color cast [24]. Owing to these characteristics, objects under uneven or chromatic illumination in a scene can be distinguished. We are now going to review the first perceptually inspired theory, the Retinex theory.

A. Retinex Theory

The basic scheme for the Retinex theory is that the intensity eyes perceive depends on the product of reflectance and illumination [12]. Hence, the basic Retinex model for each pixel x in a digital image can be written as

$$I(x) = L(x) \cdot R(x) \tag{1}$$

where, $I(x)$ is the light intensity human eyes perceive, $L(x)$ is the even or uneven distribution of the natural illumination, and $R(x)$ represents the object reflectance to the light, which is associated with the physical characteristics of object materials. Among these three variables, $I(x)$ is the only known one, and both $L(x)$ and $R(x)$ are unknown. Retinex algorithms aim to recover the lightness free of uneven illumination, like the image the HVS presents in our retinas.

Retinex generates appropriate intensity related to reflectance for a multiband image, channel by channel [12]. The intrinsic calculation procedure is composed of four steps: ratio, sequential product, reset, and average. Ratio is employed to imitate the contrast cognition of the HVS and exhibits the locality of this theory. Neighborhoods are considered through sequential products along the paths. Reset is the heart for finding the highest reflectance [25], which can be also called the local white patch (WP) [26]–[28]. Averaging the results of paths with different directions fetches up the defect of one dimension for 2-D images. The final reflectance of every point can be written as $R(x) = [\sum_{i=1}^{N} I(x)/I(x_{H_i})]/N$, where x_{H_i} is the point with the highest gray value in each path and N is the number of paths.

Given that the original image values are normalized, $0 < I(x) \leq 1$, so $I(x)/I(x_{H_i}) \geq I(x)$, we can easily prove that $R(x) \geq I(x)$ for every pixel [29]. It indicates that the result always increases the pixel values, which leads to this algorithm's defect in dealing with overbright pixels in images. The ratio-reset mechanism based on the WP assumption can be responsible for this phenomenon because WP states that at least one white object exists in every observed scene and that the ratio-reset aims to find it out.

Retinex algorithms based on WP assumption cannot avoid this defect, no matter what path selection strategies are employed. Furthermore, paths are 1-D geometrical structures, but images are 2-D and are usually sampled at discrete points. Horn proposed a 2-D version of Retinex which uses PDEs, linear systems, convolutions, and iterative solutions [30]. The four basic steps of this Retinex version are logarithms, differencing, thresholding, and summing. By using logarithms, the scheme for Retinex can be transferred as $i = l + r$ where i, l, and r are log intensity, log illumination, and log reflectance, respectively. This Retinex version extends the dynamic range of intensities for the original image, overcomes the intrinsic defect of Retinex in processing overbright pixels, and gives pleasing results. Researchers later developed several other Retinex versions to accompany Horn's idea. Blake added more suitable boundary constraints to improve the treatment of boundaries [31], and Kimmel integrated Horn's theory and some constraints into one energy function and proposed the VFR [18].

B. Variational Framework for Retinex

Based on the scheme of the Retinex theory, separating the illumination from reflectance in a given image is concluded to be an ill-posed problem, which can be solved through adding regularization items. In the image processing field, regularization has been described from both the algebraic [32] and statistical perspectives [33]. Using regularization techniques, the variational function of VFR is proposed as

$$\min\ F[l] = \int_{\Omega} \left(\|\nabla l\|_2^2 + \alpha (l-i)^2 + \beta \|\nabla (l-i)\|_2^2 \right) dxdy$$
$$\text{s.t. } l \geq i \quad \text{and} \quad \langle \nabla l, \vec{n} \rangle = 0 \quad \text{on} \quad \partial\Omega \tag{2}$$

where, Ω is the image domain, $\partial\Omega$ is its boundary, and $\vec{n}$ is the normal to the boundary. α and β are free nonnegative real parameters.

The three penalty items in the VFR force illumination spatial smoothness, the proximity between l and i, and reflectance spatial smoothness, respectively. However, reflectance is not spatially smooth in most cases, and this assumption may cause some halo artifacts.

In the VFR, the illumination is firstly estimated through the variational function, and then reflectance component is obtained by subtracting the estimated illumination from the logarithmic given image intensity. Hence, the result depends on the illumination estimation, which is the middle outcome in the procedure. That means that the final result we get may not be optimal. Therefore, this paper aims to construct a perceptually inspired variational model to recover the lightness directly and correct the uneven intensity dispersion in remote sensing images.

III. Perceptually Inspired Variational Method

A. Model Definition

Since our purpose is to adjust the intensity dispersion of an image explicitly, reducing the intensities in high-bright regions while increasing them in low-bright regions means that the energy in the image should be freshly arranged. The general energy function for an image can be expressed, as in [24], as

$$E(I) = C(I) + D(I) \tag{3}$$

where $E(I)$ is the total energy in an image, $C(I)$ represents the intensity contrast, and $D(I)$ represents the intensity dispersion. It is noted that the contrast $c(a,b)$ between two gray levels is defined as the value of $\min(a,b)$ relative to $\max(a,b)$, such as $\min(a,b)/\max(a,b)$ or $\min(a,b) - \max(a,b)$. Minimizing $E(I)$ amounts to increasing the contrast while controlling the global intensity dispersion in an even state. It can be seen that the VFR is consistent with (3). The proposed model is constructed based on the energy function.

1) Contrast Item: The intensity contrast item is proposed based on two assumptions: the environmental illumination is of spatial smoothness; and the reflectance has both features of spatial smoothness and sharpness, depending on the region. It is noted that log illumination and log reflectance share the same features as spatial illumination and reflectance.

The common prior constraints employed in a variational model can be sorted into two types: one is proposed to guarantee the image smoothness while attenuating edges and details, such as the L2 norm prior, which satisfies the Gaussian assumption of the image distribution [34]–[36]; the other is proposed to preserve edge and detailed information, such as the total variation (TV) prior [37]–[39]. However, TV favors a piecewise constant solution; therefore, it often causes staircase effects in the smooth regions while preserving the edges.

The environmental illumination varies gradually in the nature, which is considered as the major inducing factor of macro uneven intensity. Hence, we constrain it with the first kind of prior measured by the L2 norm

$$\sum_{\Omega} \|\nabla(r-i)\|_2^2 . \tag{4}$$

The reflectance reveals the true properties of the imaged objects. Remote sensing imaging objects are complicated; therefore, it is difficult to choose an appropriate prior for them. Halo artifacts are often caused by the traditional Retinex processing, which can be attributed to the inappropriate smoothness assumption of reflectance. The widely existing edges in an image are abrupt changes, which violates the previous assumption. Hence, halo artifacts usually occur at the juncture of edges and nonedges in the partion of the result that was under dark fog before. Therefore, it is reasonable to propose multiprior to the reflectance according to the image contents. Primarily, the TV prior and the L2 norm prior are arranged to the edges and nonedges, respectively

$$\sum_{\Omega} \|\nabla r\|_t^t , \quad \text{where} \quad t = \begin{cases} 1, & \text{if } x \in Edges \\ 2, & \text{if } x \in Non\text{-}edges \end{cases} \tag{5}$$

where x represents a pixel in an image. The usual way to distinguish edges and nonedges is based on edge extraction relying on the threshold setting, which varies according to different images. Hence, it is necessary to select the threshold value adaptively. For an image, we cannot determine the exact threshold value visually but can estimate the percentage of edge or nonedge information approximately. Hence, the problem of setting the absolute value is first converted into the relative percentage setting, which can be calculated statistically. An image cumulative histogram reveals the cumulative percentage that each intensity level takes up in an image. Hence, the second step is to determine the according intensity value through the image cumulative histogram. Given that the gradient image I_G represents the edge information of the original image, the percentage parameter is p, and the intensity value corresponding to p in the cumulative histogram is I_{Gp}, if $I_G(x) > I_{Gp}$ then $x \in Edges$, else $x \in Non\text{-}edges$. Thus, p percent of image contents are constrained by the TV prior, and $(1-p)$ percent are constrained by the L2 norm prior.

Hence, the contrast item of r can be expressed as

$$C(r) = \alpha_C \sum_{\Omega} \|\nabla(r-i)\|_2^2 + \beta_C \sum_{\Omega} \|\nabla r\|_t^t \tag{6}$$

where $t = \begin{cases} 1, & \text{if } x \in Edges \\ 2, & \text{if } x \in Non\text{-}edges \end{cases}$, α_C and β_C are nonnegative free parameters weighting the above items, respectively.

2) Dispersion Item: There are several possible choices for the dispersion control item, such as attachment to original data, attachment to the average value, assumed to be 1/2 for normalized data, and the linear combination of the above two. In principle, to measure the dispersion, any distance function can be used. The simplest example would be a quadratic distance.

In the uniform variational models for HE and automatic color enhancement, attachment to the average value is employed as the dispersion control item [23]; while the VFR employs the attachment to original data item to control the illumination dispersion. It is noted that attachment to the average value sometimes leads to overcontrast, so that the linear combination of these two kinds of constraints is often adopted. However, since the contrast can be well controlled in our model by the

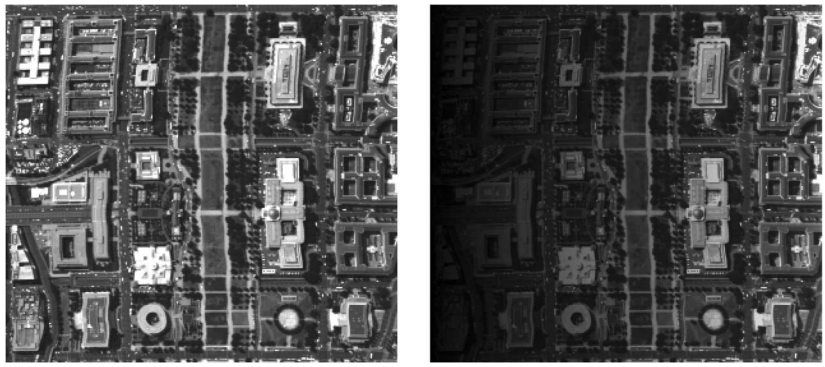

Fig. 1. Single-band images. (a) Original image. (b) Horizontally degraded image.

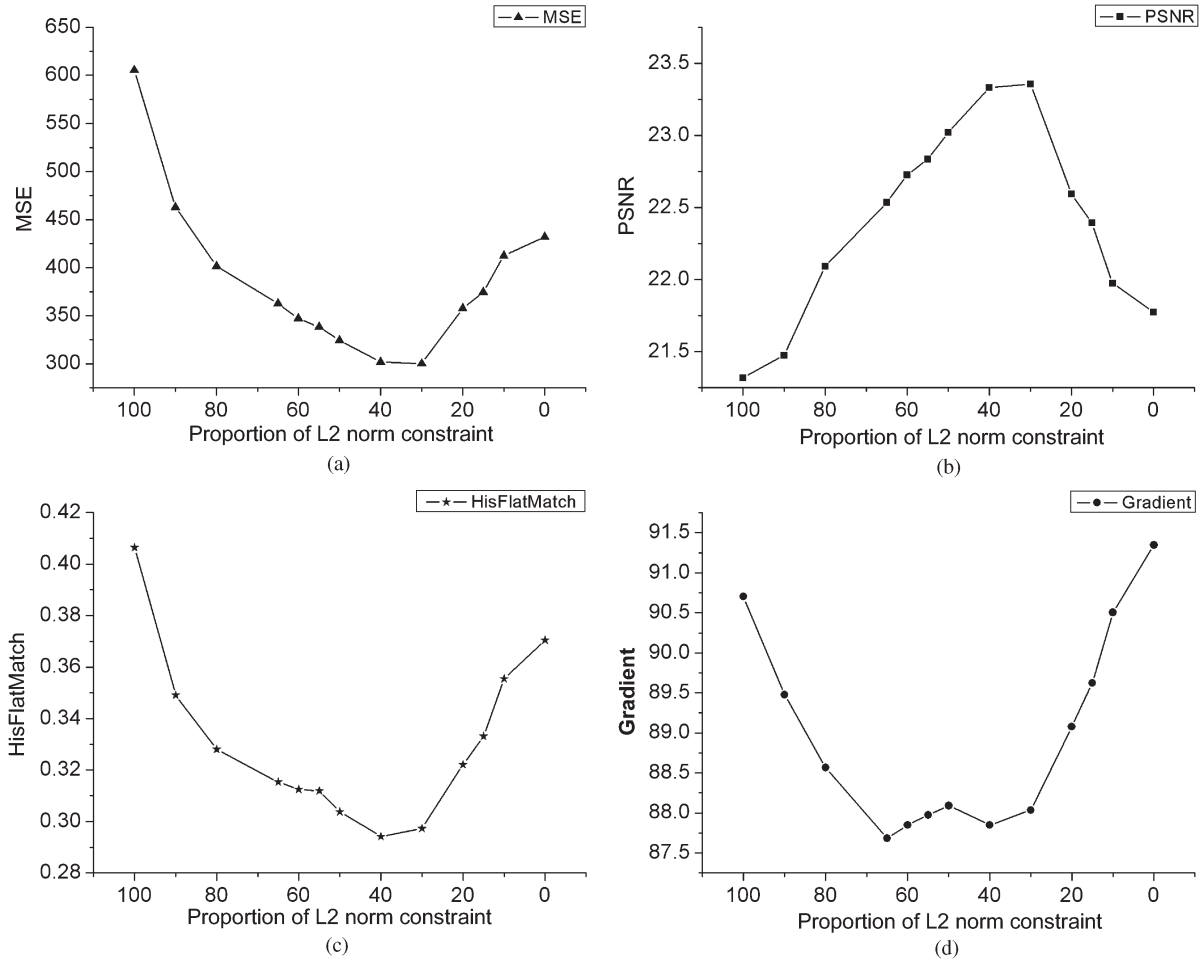

Fig. 2. Quantitative assessment of percentage parameter. (a) MSE. (b) PSNR. (c) HFM. (d) gradient.

contrast item that is adaptive to the regions, only the attachment to the average value is used as the dispersion item. Moreover, considering the physical characteristics of reflectance in the spatial domain, we suppose that R is normalized $0 \leq R \leq 1$, in other words, $L \geq I$ and $r \leq 0$. This assumption overcomes the traditional Retinex defect in processing overexposed regions owing to its WP mechanism. In addition, the attachment to average value can be interpreted by the "gray world" (GW) assumption [28], which says that the average channel color intensity in every observed scene is perceived as the middle gray. Overall, we constrain the spatial reflectance R as $(R - 1/2)^2$, and this can be translated into the logarithmic domain as $[\exp(r) - 1/2]^2$. Consequently, the dispersion item of r can be written as

$$D(r) = \beta_D \sum_{\Omega} [\exp(r) - 1/2]^2, \quad r \leq 0. \tag{7}$$

3) Correction Model: By integrating the contrast and dispersion items in an energy function, we tentatively put forward

TABLE I
QUANTITATIVE ASSESSMENT

	MSE	PSNR	Mean	Gradient	HFM
Original image	0	$+\infty$	94.04	81.97	0
Degraded image	4202.10	11.90	46.08	40.78	0.904
Mask	1217.41	17.27	86.87	40.47	0.668
VFR	441.54	21.68	107.46	84.40	0.371
Proposed method	300.28	23.36	104.26	88.04	0.297

(a) (b) (c)

Fig. 3. Corrected results of three methods. (a) Mask filtering. (b) VFR. (c) Proposed method.

the perceptually inspired variational model about r as

$$\min\ F[r] = \sum_{\Omega} \Big(\|\nabla(r-i)\|_2^2 + \lambda_1 \|\nabla r_t\|_t^t + \lambda_2 \left[\exp(r) - 1/2\right]^2 \Big)$$
$$t = \begin{cases} 1, & \text{if } x \in Edges \\ 2, & \text{if } x \in Non\text{-}edges \end{cases}, \quad \text{s.t. } r(x) \le 0 \quad (8)$$

where $\lambda_1 := \beta_C/\alpha_C$ and $\lambda_2 := \beta_D/\alpha_C$ are nonnegative parameters to control the contribution of the second and the third items in (8), respectively.

B. Numerical Solution

The minimization for $F[r]$ can be referred as an optimal problem; thus, we consider its Euler–Lagrange equation written as

$$\delta F(r) = \frac{\partial F}{\partial r} = -\Delta(r-i) - \lambda_1 \cdot \left(\nabla \left(\frac{\nabla r_1}{|\nabla r_1|} + 2\Delta r_2 \right) \right) + \lambda_2 \cdot 2\exp(r)\left[\exp(r) - 1/2\right] = 0 \quad (9)$$

where Δ is the Laplacian operator, which can be approximated by a linear convolution with the kernel $[0\ 1\ 0; 1\ -4\ 1; 0\ 1\ 0]$. Since our equation involves both linear and nonlinear problems, we intend to choose the classic steepest descent method to solve it. In addition, the steepest descent solution of the Laplacian operator is a Gaussian smoothing operation with increasing variance of the initial condition. This explains why Jobson *et al.* [16], [17] proposed to reconstruct the illumination by Gaussian smoothing and reflects the locality of the L2 norm prior. The L2 norm prior is isotropic, whereas the TV is anisotropic, so that edges with a certain direction in a local region can be preserved efficiently. Generally, the contrast item in the proposed model performs the locality of human vision. Based on the steepest decent method, the above problem is transformed to solve the following equation:

$$\frac{\partial r}{\partial t} = -\delta F(r). \quad (10)$$

When discretized with respect to parameter t, the above equation can be written as

$$\frac{r^{k+1} - r^k}{\Delta t} = \Delta(r-i) + \lambda_1 \cdot \left(\nabla \left(\frac{\nabla r_1}{|\nabla r_1| + \xi} + 2\Delta r_2 \right) \right) - \lambda_2 \cdot 2\exp(r)\left[\exp(r) - 1/2\right] \quad (11)$$

where Δt is the setting constant as the iteration step length, $\Delta t \ge 0$, and ξ is a constant avoiding the denominator to be 0. Hence, the iteration equation can be expressed as

$$r^{k+1} = r^k + \Delta t \cdot G \quad (12)$$
$$G = \Delta(r-i) + \lambda_1 \cdot \left(\nabla \left(\frac{\nabla r_1}{|\nabla r_1| + \xi} + 2\Delta r_2 \right) \right) - \lambda_2 \cdot 2\exp(r)\left[\exp(r) - 1/2\right]. \quad (13)$$

The iteration will not stop until the terminal condition is satisfied. This is a time-consuming process due to the image size. For a 1000 $\times$ 1000 image, about 10 min is needed to achieve a satisfactory resolution. However, there is room for an improvement in efficiency by using some advanced mathematical optimization method, and this is the subject of our further work.

IV. EXPERIMENTS

The proposed method was validated by applying it to remote sensing images. To evaluate the results quantitatively, experiments on synthetic data are firstly carried out. Then, real remote sensing images are utilized to test the proposed method.

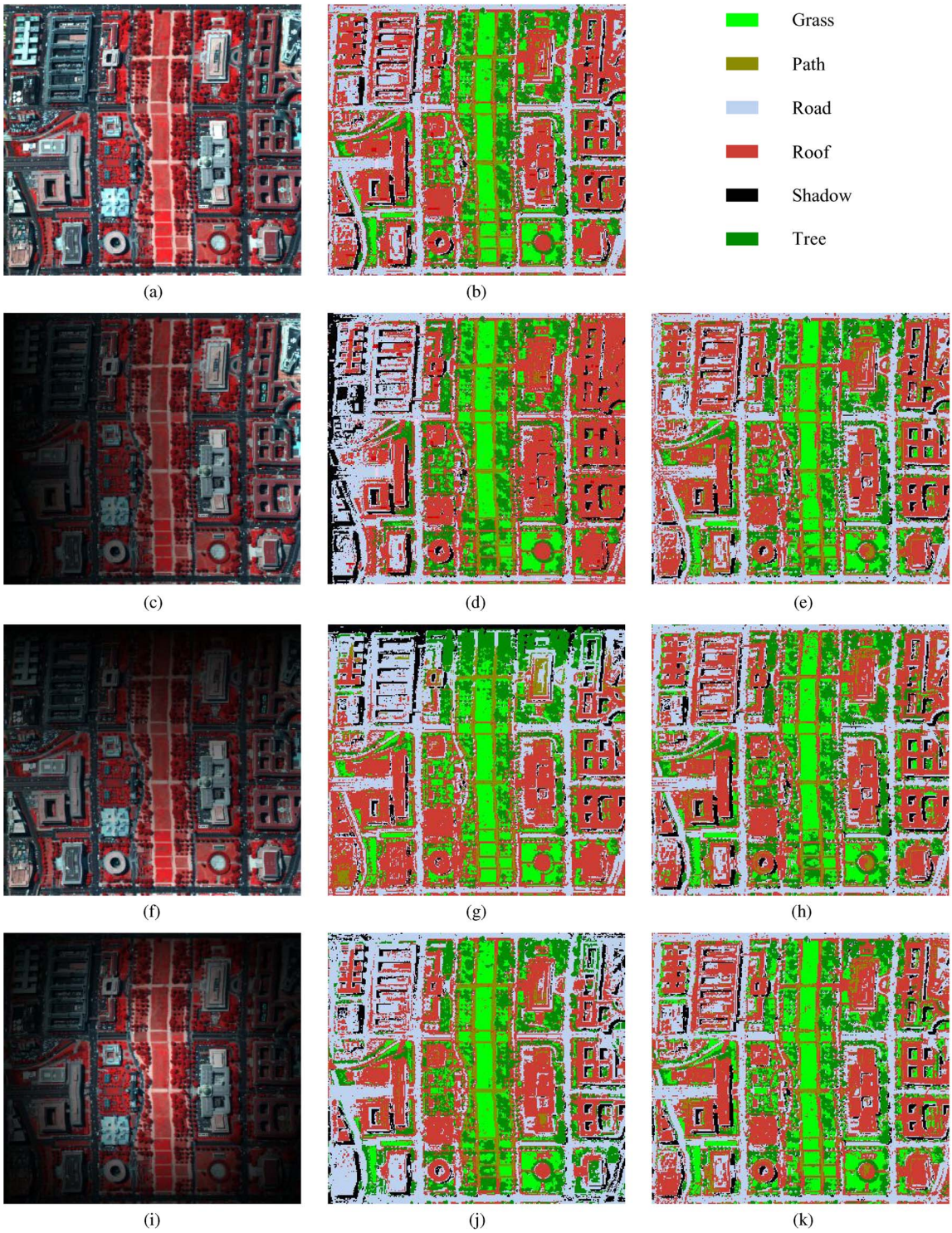

Fig. 4. Multiband degraded images and classification images. (a) Original image, (b) classification image of (a), (c) horizontally degraded image, (d) classification image of (c), (e) classification image of the corrected result of (c), (f) vertically degraded image (g), classification image of (f), (h) classification image of the corrected result of (g), (i) Gaussian degraded image (j) classification image of (i), (k) classification image of the corrected result of (i).

A. Experiments on Synthetic Data

A remote sensing image with high quality from Washington DC acquired by the HYDICE sensor was chosen as the original standard image. This image has 210 bands and a 5-m spatial resolution. We selected a 307 $\times$ 280 subset and four bands from the original whole image for the subsequent synthetic experiments. Although the parameters λ_1, λ_2, and Δt should vary in terms of specific images, overall good results with the following set were found: $\Delta t = 0.075$, $\lambda_1 = 0.02$, and $\lambda_2 = 0.01$. For the proportion parameter p, the optimal value was determined through testing a series of different proportions on one selected single-band image shown as Fig. 1(a). It was horizontally degraded, as the following test data shows in Fig. 1(b).

TABLE II
CLASSIFICATION ACCURACY AND KAPPA COEFFICIENT

		Horizontal	Vertical	Gaussian	Original image
Classification accuracy	The degraded image	78.47%	71.78%	78.36%	88.97%
	The corrected image	87.53%	84.73%	85.68%	
Kappa coefficient	The degraded image	0.7166	0.6385	0.7201	0.8523
	The corrected image	0.8330	0.7959	0.8085	

Now, we will discuss the influence of the percentage parameter p to the final result. According to the parameter selecting strategy described in Section 3-A, p is manually tuned in the set $\mathbf{P} = \{100, 90, 80, 65, 60, 55, 50, 40, 30, 20, 15, 10, 0\}\%$. When p equals 100%, it means that the L2 norm totally constrains r. On the contrary, when p equals 0%, the TV totally constrains r. Several factors, including MSE, PSNR, HFM (histogram flatness match), and gradient, are introduced to make quantitative assessments to the results

$$MSE = E\left((\hat{I} - I)^2\right) \tag{14}$$

$$PSNR = 10 \times \log\left(\frac{255^2}{MSE}\right) \tag{15}$$

$$HFM = \frac{1}{N}\sum_{I=0}^{255}\left|H(\hat{I}) - H(I)\right| \tag{16}$$

and (17), shown at the bottom of the page, where $\hat{I}$ is the estimated value, I is the original vale, N is the size of the image, $H(I)$ represents the frequency of intensity value I, and G is the maximum of the gradients in four directions $G = \max(G_{H,}G_{V,}G_{D,}G_{rD})$. The lower HFM corresponds to a better match of the result to the original image. As smooth light is removed from the image, the result usually contains high-frequency information with a high gradient. If appropriate prior constrain different regions, the result should have an appropriate gradient higher than the degraded and lower than the overenhanced.

Fig. 2 shows the curves of different assessment factors versus the percentage parameter p. The following conclusions are drawn: First, the multiprior constraint outperforms the solitary constraint, either L2 norm or TV. Second, consulting Table I and Fig. 2(d), we found that all the results had higher gradient values than the original image, which means that the proposed algorithm enhances the high-frequency information, as well as weakens the low-frequency information. However, the multiprior constraint yields relatively satisfying results. It suggests that associating prior type with image content is reasonable and effective. Finally, integrating the assessment with the four factors, $p = 30\%$ is employed as the percentage setting in the following tests for the Washington DC image.

Fig. 3 shows the corrected results of the mask, the VFR, and the proposed method. The intensity dispersion in the three results is all corrected to an even level. However, Fig. 3(b) and (c) shows a more pleasing visual effect than Fig. 3(a) does. Fig. 3(a) is blurred after the uneven illumination is wiped off because the simple subtract operation in the mask method reduces the amount of information in images without fully considering spatial features and correlations. The brightness of Fig. 3(c) is lower than in Fig. 3(b) and is closer to the original image. This is attributed to the dispersion item in the proposed model, which restricts the intensity attachment to the middle gray and avoids overexposure in the result. In addition, Fig. 3(b) is likely to be covered in mist, whereas Fig. 3(c) shows clear edges and details owing to the TV prior constraint, which eliminates the halo artifacts. Table I presents the quantitative assessment results of these three methods, in which the proposed method outperforms the mask and the VFR.

To test the effectiveness of the proposed method further, it was applied to process multiband images with three different types of degradation: horizontal, vertical, and Gaussian. Fig. 4(c), (f), and (i) show the degraded images. The multiband images were processed band by band. The four selected bands are distributed in red, green, blue, and the near infrared spectral range, respectively. Classification results of degraded and corrected images by MLC were adopted to assess the correction effects via the overall classification accuracies and kappa coefficients. The parameter setting in this test is coherent with the single-band test. In terms of visual assessment, the classification maps of the corrected images are better than those of the degraded images, particularly the darker and brighter regions. Quantitatively, Table II presents the overall accuracy and kappa coefficients, which are both improved in the classification maps of the images corrected by the proposed method. However, the classification maps of the corrected images appear more cracked than in Fig. 4(b), which is attributed to the increased gradients of the processed images. In summary, whether from qualitative or quantitative assessment, it can be concluded that the proposed method can efficiently remove the influence of

$$Gradient = \frac{1}{N}\sum\sqrt{(G - G_H)^2 + (G - G_V)^2 + (G - G_D)^2 + (G - G_{rD})^2} \tag{17}$$

Fig. 5. Results of the aerial data I. (a) Original aerial image. (b) VFR. (c) The proposed method.

uneven light, explore the valid information, and enhance the details in images.

B. Experiments on Real Aerial Remote Sensing Images

In this section, the proposed method is applied to real aerial remote sensing images. Fig. 5(a) shows the first experimental

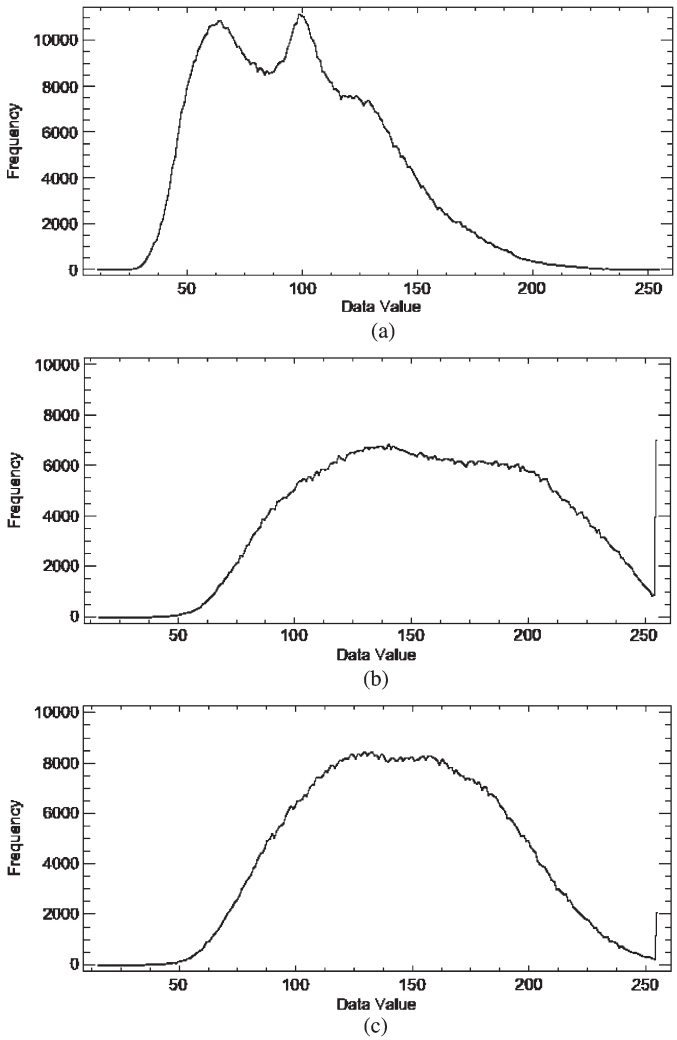

Fig. 6. Histograms of Fig. 5(a)–(c).

data size of 1000 × 1000 pixels, in which the brightness of the left and top buildings is brighter than that of the right and bottom buildings, due to the uneven distribution of environmental light. As no references are available for real remote sensing images, it is hard to select the most appropriate parameters and assess the results quantitatively. Parameters were adjusted manually, consulting the setting in the synthetic test. For the first data, parameters were set as $\Delta t = 0.075$, $\lambda_1 = 0.02$, $\lambda_2 = 0.01$, and $p = 50\%$.

The comparison between the proposed method and the VFR was carried out, as shown in Fig. 5(b) and (c). Results indicate that both the VFR and the proposed method can remove the uneven brightness distribution in the original image visually, but some regions in Fig. 5(b) are overexposed after processing, while in Fig. 5(c), this phenomenon is eliminated. Objectively, from the histograms shown in Fig. 6, it is seen that (b) and (c) are flatter than (a), but there is a leap in the tail of (b), which is responsible for the overexposed phenomenon in Fig. 5(b), whereas (c) has high similarity with Gaussian distribution.

Fig. 7 shows four detailed regions cropped from Fig. 5(a)–(c). Two regions in the first line are bright before, and the corrected results decline their intensities. The other

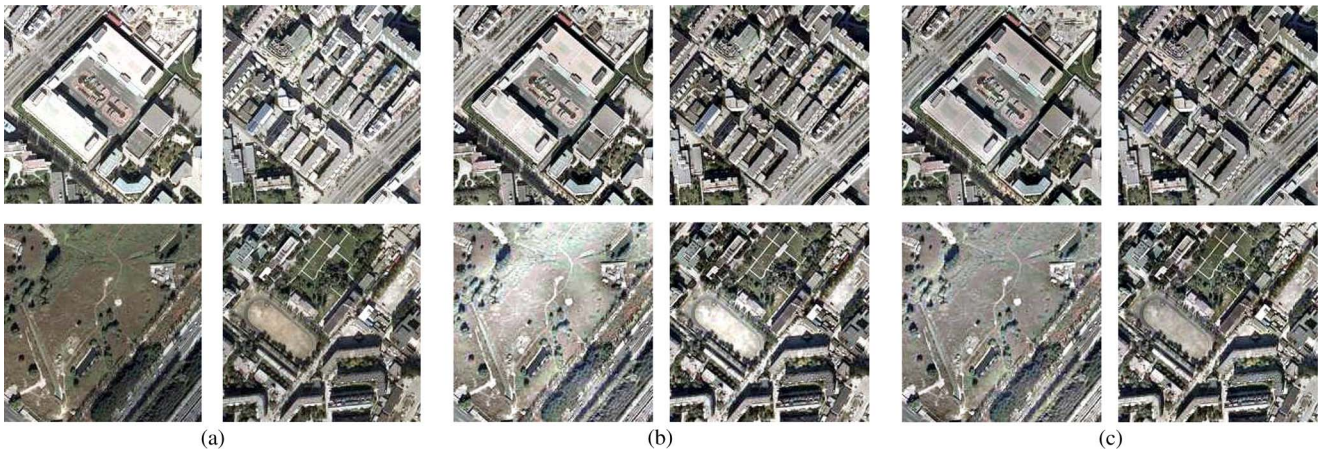

Fig. 7. Detailed regions cropped from Fig. 5(a)–(c).

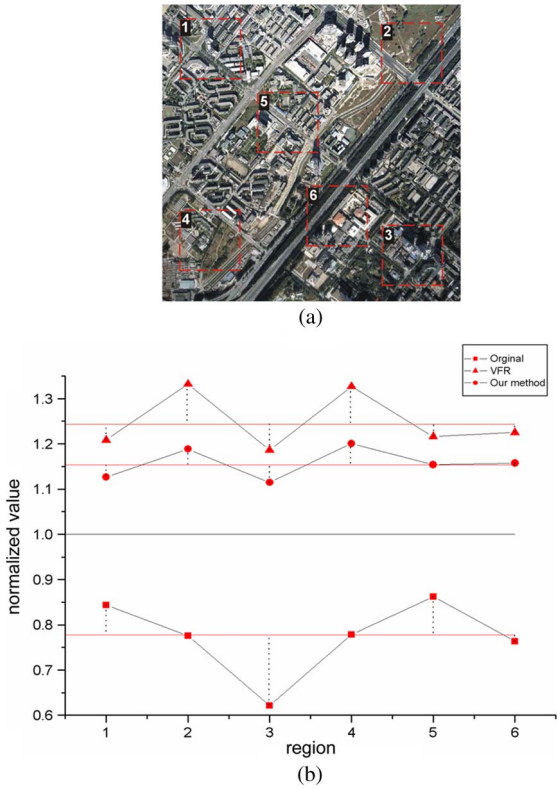

Fig. 8. Six selected regions and their means. (a) Six regions. (b) Broken lines with the means of six regions for three images in Fig. 5.

two detailed regions in the second line are dark before and are enhanced in the corrected results but overexposed in the VFR, as shown in Fig. 7(b). This is attributed to the third item in the proposed method, which controls the macro intensity dispersion and ensures the whole visual performance.

For quantitative assessment, six regions were cropped from the original image, as shown in Fig. 8(a), and their normalized means in one band were compared. In Fig. 8(b), the middle line crossing value 1 represents the ideal mean value. The other three parallel lines from bottom to top correspond to the means of the original image, the corrected images processed by the proposed method, and the VFR. The points around these

Fig. 9. Results of real data II. (a) Original aerial image. (b) VFR. (c) The proposed method.

Fig. 9. *(Continued).* Results of real data II. (d)–(f) Detailed region 1 cropped from (a)–(c). (g)–(i) Detailed region 2 cropped from (a)–(c). (j)–(l) Detailed region 3 cropped from (a)–(c).

lines correspond to those six region means, and the distances from these points to their mean line reflect the even degree of brightness. In Fig. 8(b), points in the second broken line have the shortest distances among the three broken lines, which indicate that the final image corrected by the proposed method has the highest even degree.

Results of the second data with a size of 950 $\times$ 600 and the third data with a size of 600 $\times$ 400 are shown in Figs. 9 and 10. Parameters were set as $\Delta t = 0.075$, $\lambda_1 = 0.001$, $\lambda_2 = 0.01$, and $p = 50\%$. Nine bright regions were cropped from the second data and shown in Fig. 9(d)–(l). Lightness in the middle column is not darker or even brighter than that in the left, whereas image in the right column shows an even tone with the lightness of bright areas declining. These results indicate that out method outperforms the VFR in handling those originally bright areas. The region in the third line of Fig. 10 is also a bright area, whose lightness has tremendous decline in the result of the right column comparing with the left and middle columns. Lightness in Fig. 10(e) is raised, but the color is distorted a little. Fig. 10(f) is more satisfactory visually. Generally, results demonstrate the effectiveness of our method in dealing with both dark and bright regions.

Finally, we intend to discuss the convergence of the proposed method thorough analyzing the relative iteration error with the iteration number. From the convergence curves shown in Fig. 11, it can be seen that this method can quickly converge to a stable-state solution with a few steps.

V. Conclusion

A variational method has been presented for correcting uneven intensity in remote sensing images, using multi priors (L2 norm and TV) as the contrast item and GW as the dispersion item. Synthetic and real remote sensing images were used to validate this method, and the performances were evaluated both subjectively and objectively. The experimental results show that corrected images by the proposed method have an even intensity and maintain the original chrominance. Compared with the VFR, our method avoids the overexposure phenomenon and halo artifacts owing to the effective items in the energy function. As with the VFR, the proposed method is time consuming and the parameters weighting each item are determined manually. We will investigate a fast algorithm and automatic parameter selection in our future work.

(a)

(b)

(c)

Fig. 10. Results of real data III. (a) Original aerial image. (b) VFR. (c) The proposed method.

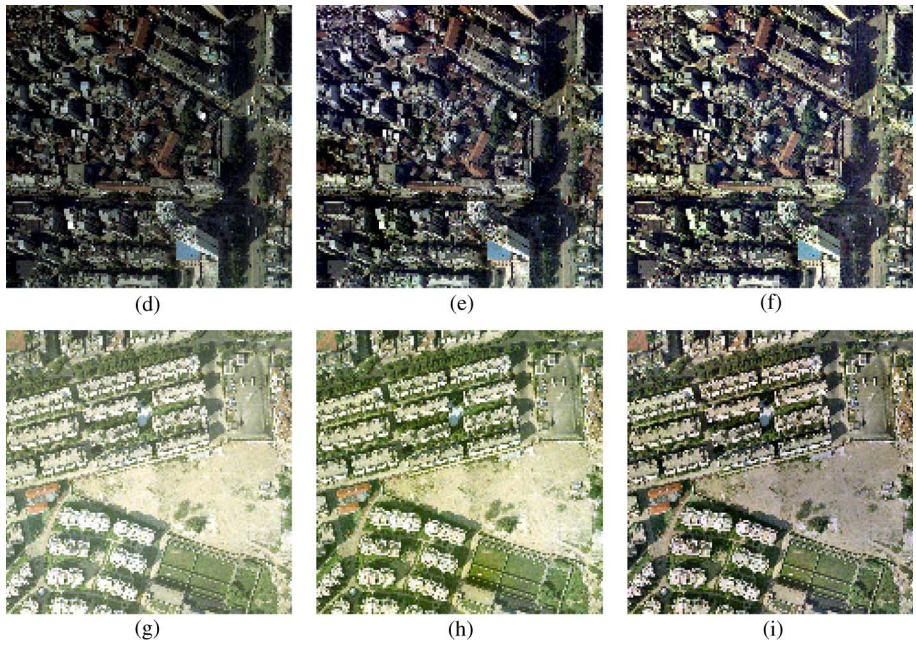

Fig. 10. *(Continued).* Results of real data III. (d)–(f) Detailed region 1 cropped from (a)–(c). (g)–(i) Detailed region 2 cropped from (a)–(c).

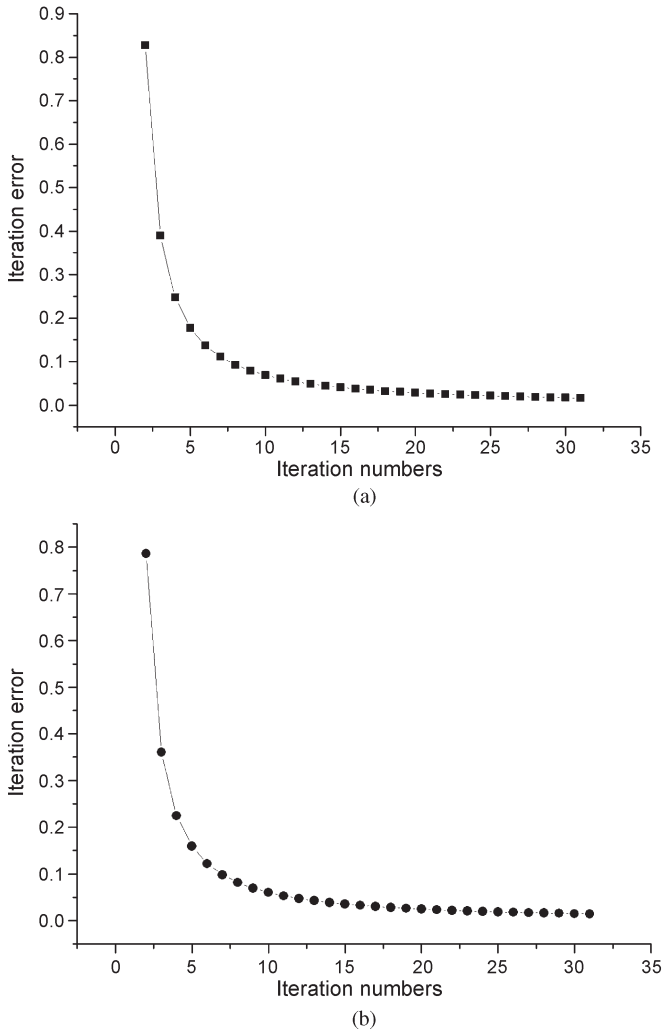

Fig. 11. Convergence curves. (a) Convergence curve for the synthetic image. (b) Convergence curve for the aerial data I.

REFERENCES

[1] C. Coll, J. M. Galve, J. M. Sanchez, and V. Caselles, "Validation of Landsat-7/ETM+ thermal-band calibration and atmospheric correction with ground-based measurements," *IEEE Trans. Geosci. Remote Sens.*, vol. 48, no. 1, pp. 547–555, Jan. 2010.

[2] S. R. Pudale and U. V. Bhosle, "Comparative study of relative radiometric normalization techniques for resourcesat1 LISS III sensor images," in *Proc. ICCIMA*, 2007, vol. 3, pp. 233–239.

[3] H. Yeganeh and A. Z. A. Rezaie, "A novel approach for contrast enhancement based on histogram equalization," in *Proc. Int. Conf. Comput. Commun. Eng.*, 2008, pp. 256–260.

[4] M. Kim and M. G. Chung, "Recursively separated and weighted histogram equalization for brightness preservation and contrast enhancement," *IEEE Trans. Consum. Electron.*, vol. 54, no. 3, pp. 1389–1397, Aug. 2008.

[5] H. K. C. N. Sengee, "Brightness preserving weight clustering histogram equalization," *IEEE Trans. Consum. Electron.*, vol. 54, no. 3, pp. 1329–1337, Aug. 2008.

[6] C. Wang and Z. Ye, "Brightness preserving histogram equalization with maximum entropy: A variational perspective," *IEEE Trans. Consum. Electron.*, vol. 51, no. 4, pp. 1326–1334, Nov. 2005.

[7] S. Sarkar and G. Healey, "Hyperspectral texture synthesis using histogram and power spectral density matching," *IEEE Trans. Geosci. Remote Sens.*, vol. 48, no. 5, pp. 2261–2270, May 2010.

[8] H. J. Kaufman and M. A. Sid-Ahmed, "Hardware realization of a 2D IIR semisystolic filter with application to real-time homomorphic filtering," *IEEE Trans. Circuits Syst. Video Technol.*, vol. 3, no. 1, pp. 2–14, Feb. 1993.

[9] U. Nnolim and P. Lee, "Homomorphic filtering of colour images using a spatial filter Kernel in the HSI colour space," in *Proc. IEEE Int. Instrum. Meas. Technol. Conf.*, 2008, pp. 1738–1743.

[10] M. J. Seow and V. K. Asari, "Homomorphic processing system and ratio rule for color image enhancement," in *Proc. IEEE Int. Joint Conf. Neural Netw.*, 2004, vol. 4, pp. 2507–2511.

[11] M. Wang and J. Pan, "A method of removing the uneven illumination for digital aerial image," *J. Image Graph.*, vol. 9, no. 6, pp. 744–748, 2004.

[12] E. H. Land and J. J. McCann, "Lightness and Retinex theory," *J. Opt. Soc. Amer.*, vol. 61, no. 1, pp. 1–11, Jan. 1971.

[13] E. H. Land, "The Retinex theory of color vision," *Sci. Amer.*, vol. 237, no. 6, pp. 108–128, Dec. 1977.

[14] D. Marini and A. Rizzi, "A computational approach to color adaptation effects," *Image Vis. Comput.*, vol. 18, no. 13, pp. 1005–1014, Oct. 2000.

[15] T. J. Cooper and F. A. Baqai, "Analysis and extensions of the Frankle-McCann Retinex algorithm," *J. Electron. Imag.*, vol. 13, no. 1, pp. 85–92, Jan. 2004.

[16] D. J. Jobson, Z.-U. Rahman, and G. A. Woodell, "Properties and performance of a center/surround Retinex," *IEEE Trans. Image Process.*, vol. 6, no. 3, pp. 451–462, Mar. 1997.
[17] D. J. Jobson, Z.-U. Rahman, and G. A. Woodell, "A multiscale Retinex for bridging the gap between color images and the human observation of scenes," *IEEE Trans. Image Process.*, vol. 6, no. 7, pp. 965–976, Jul. 1997.
[18] R. Kimmel, M. Elad, D. Shaked, K. Keshet, and I. Sobel, "A variational framework for Retinex," *Int. J. Comput. Vis.*, vol. 52, no. 1, pp. 7–23, Apr. 2003.
[19] E. Provenzi, M. Fierro, A. Rizzi, L. D. Carli, D. Gadia, and D. Marini, "Random spray Retinex: A new Retinex implementation to investigate the local properties of the model," *IEEE Trans. Image Process.*, vol. 16, no. 1, pp. 162–171, Jan. 2007.
[20] T. F. Chan and J. Shen, *Image Processing and Analysis: Variational, PDE, Wavelet, and Stochastic Methods*. Philadelphia, PA: Soc. Ind. Math., 2005.
[21] Y. Wang, R. Niu, L. Zhang, and H. Shen, "Region-based adaptive anisotropic diffusion for image enhancement and denoising," *Opt. Eng.*, vol. 49, no. 11, pp. 117 007-1–117 007-19, Nov. 2010.
[22] Q. Yuan, L. Zhang, H. Shen, and P. Li, "Adaptive multiple-frame image super-resolution based on U-curve," *IEEE Trans. Image Process.*, vol. 19, no. 12, pp. 3157–3170, Dec. 2010.
[23] M. Bertalmio, V. Caselles, E. Provenzi, and A. Rizzi, "Perceptual color correction through variational techniques," *IEEE Trans. Image Process.*, vol. 16, no. 4, pp. 1058–1072, Apr. 2007.
[24] R. Palma-Amestoy, E. Provenzi, M. Bertalmio, and V. Caselles, "A perceptually inspired variational framework for color enhancement," *IEEE Trans. Pattern Anal. Mach. Intell.*, vol. 31, no. 3, pp. 458–474, Mar. 2009.
[25] M. Bertalmio, V. Caselles, and E. Provenzi, "Issues about Retinex theory and contrast enhancement," *Int. J. Comput. Vis.*, vol. 83, no. 1, pp. 101–119, Jun. 2009.
[26] A. Rizzi, C. Gatta, and D. Marini, "A new algorithm for unsupervised global and local color correction," *Pattern Recognit. Lett.*, vol. 24, no. 11, pp. 1663–1677, Jul. 2003.
[27] A. Rizzi, "From Retinex to automatic color equalization: Issues in developing a new algorithm for unsupervised color equalization," *J. Electron. Imag.*, vol. 13, no. 1, pp. 75–84, Jan. 2004.
[28] E. Provenzi, C. Gatta, M. Fierro, and A. Rizzi, "A spatially variant white-patch and gray-world method for color image enhancement driven by local contrast," *IEEE Trans. Pattern Anal. Mach. Intell.*, vol. 30, no. 10, pp. 1757–1770, Oct. 2008.
[29] E. Provenzi, L. D. Carli, and A. Rizzi, "Mathematical definition and analysis of the Retinex algorithm," *J. Opt. Soc. Amer. A, Opt. Image Sci.*, vol. 22, no. 12, pp. 2613–2621, Dec. 2005.
[30] B. K. P. Horn, "Determining lightness from an image," *Comput. Vis. Graph.*, vol. 3, no. 4, pp. 277–299, Dec. 1974.
[31] A. Blake, "Boundary conditions for lightness computation in Mondrian world," *Comput. Vis. Graph.*, vol. 32, no. 3, pp. 314–327, Dec. 1985.
[32] M. K. Ng, H. Shen, L. Zhang, and E. Lam, "A total variation based super-resolution reconstruction algorithm for digital video," *EURASIP J. Adv. Signal Process.*, vol. 2007, 2007, Article ID 74585.
[33] H. Shen, L. Zhang, B. Huang, and P. Li, "A MAP approach for joint motion estimation, segmentation, and super resolution," *IEEE Trans. Image Process.*, vol. 16, no. 2, pp. 479–490, Feb. 2007.
[34] S. Farsiu, M. D. Robinson, M. Elad, and P. Milanfar, "Fast and robust multiframe super resolution," *IEEE Trans. Image Process.*, vol. 13, no. 10, pp. 1327–1344, Oct. 2004.
[35] H. Fu, M. K. Ng, M. Nikolova, and J. L. Barlow, "Efficient minimization methods of mixed L2-L1 and L1-L1 norms for image restoration," *SIAM J. Sci. Comput.*, vol. 27, no. 6, pp. 1881–1902, 2006.
[36] B. Du and L. Zhang, "Random selection based anomaly detector for hyperspectral imagery," *IEEE Trans. Geosci. Remote Sens.*, vol. 49, no. 5, pp. 1578–1589, May 2011.
[37] L. I. Rudin, S. Osher, and E. Fastemi, "Nonlinear total variation based noise removal algorithms," *Phys. D*, vol. 60, pp. 259–268, 1992.
[38] L. Zhang, Q. Yuan, H. Shen, and P. Li, "Muti-frame image super-resolution adapted with local spatial information," *J. Opt. Soc. Amer.*, vol. 28, no. 3, pp. 381–390, Mar. 2011.
[39] M. K. Ng, H. Shen, S. Chaudhuri, and A. C. Yau, "Zoom-based super-resolution reconstruction approach using prior total variation," *Opt. Eng.*, vol. 46, no. 12, p. 127 003, Dec. 2007.

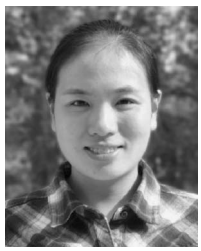

Huifang Li received the B.S. degree in geographical information science from the China University of Mining and Technology, Xuzhou, China, in 2008. She is currently working toward the Ph.D. degree at the State Key Laboratory of Information Engineering in Surveying, Mapping, and Remote Sensing, Wuhan University, Wuhan, China.

Her research interests include variational methods, image processing, and dehazing and deshadowing of remote sensing images.

Liangpei Zhang (M'06–SM'08) received the B.S. degree in physics from Hunan Normal University, ChangSha, China, in 1982, the M.S. degree in optics from the Xi'an Institute of Optics and Precision Mechanics of Chinese Academy of Sciences, Xi'an, China, in 1988, and the Ph.D. degree in photogrammetry and remote sensing from Wuhan University, Wuhan, China, in 1998.

He is currently with the State Key Laboratory of Information Engineering in Surveying, Mapping, and Remote Sensing, Wuhan University, as the Head of the Remote Sensing Division. He is also a "Chang-Jiang Scholar" Chair Professor appointed by the Ministry of Education, China. He has more than 230 research papers and five patents. He is currently Principal Scientist for the China State Key Basic Research Project (2011–2016) appointed by the Ministry of National Science and Technology of China to lead the remote sensing program in China. His research interests include hyperspectral remote sensing, high-resolution remote sensing, image processing, and artificial intelligence.

Dr. Zhang regularly serves as a Co-Chair of the series SPIE Conferences on Multispectral Image Processing and Pattern Recognition, Conference on Asia Remote Sensing, and many other conferences. He edits several conference proceedings, issues, and the Geoinformatics Symposiums. He also serves as an Associate Editor of the *International Journal of Ambient Computing and Intelligence*, the *International Journal of Image and Graphics*, the *International Journal of Digital Multimedia Broadcasting*, the *Journal of Geo-spatial Information Science*, and the *Journal of Remote Sensing*. He is Fellow of IEE, Executive Member (Board of Governor) of the China National Committee of International Geosphere-Biosphere Programme, Executive Member for the China Society of Image and Graphics, and others.

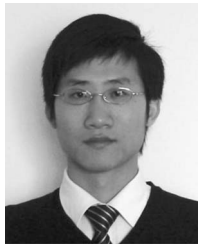

Huanfeng Shen (M'10) received the B.S. degree in surveying and mapping engineering and the Ph.D. degree in photogrammetry and remote sensing from Wuhan University, Wuhan, China, in 2002 and 2007, respectively.

In July 2007, he joined the School of Resources and Environmental Science, Wuhan University, where he is currently an Associate Professor. His current research interests include image processing, remote sensing applications, data fusion, and data assimilation